J. Fluid Mech. (1977), *vol.* 80, *part* 2, *pp.* 369–391
Printed in Great Britain

The collapse of a non-hemispherical bubble attached to a solid wall

By A. SHIMA AND K. NAKAJIMA
Institute of High Speed Mechanics, Tōhoku University, Sendai, Japan

(Received 25 March 1976 and in revised form 10 September 1976)

The problem of the collapse of a vapour/gas bubble attached to a solid wall and initially perturbed from a hemispherical shape is solved numerically by the variational method, in which the bubble's viscosity and compressibility in liquid are neglected. The effects of surface tension on the collapsing bubble are taken into account. The rebounding processes of a non-hemispherical gas bubble are simulated: the gas inside the bubble undergoes an adiabatic process. The results of numerical calculations are given for two initial shapes: one is close to a prolate spheroid, the other is close to an oblate spheroid. The governing equations for the motion of a bubble can be written in matrix form, which is simpler than that derived from perturbation theory. This analysis using the variational method may be applied to more complicated problems.

1. Introduction

Minute nuclei containing undissolved gas and/or vapour in liquid grow in regions of low pressure and cause cavitation. Cavitation damage results from the collapse of these bubbles in regions of high pressure. Therefore studies of the mechanism of cavitation damage have mostly been concerned with explaining the destructive action brought about by the collapse of a bubble. Rayleigh (1917) solved the problem of the collapse of a spherical bubble in a homogeneous, inviscid, incompressible liquid under a constant ambient pressure. His analysis suggests that cavitation damage is due to the high pressures developed near a spherical cavity.

From their observations of the behaviour of a cavitation bubble produced by a magnetostriction oscillator, however, Kornfeld & Suvorov (1944) found that cavities could not retain a spherical or hemispherical shape in the course of their collapse, as Rayleigh's theory had assumed, since they very easily lost stability of shape. Consequently, Kornfeld & Suvorov suggested that the impact of liquid jets formed during the collapse of cavitation bubbles might be responsible for cavitation damage.

As to the stability of the spherical shape of a vapour cavity, Plesset (1954) and Plesset & Mitchell (1955) demonstrated for the collapsing cavity that, as the mean radius R approaches zero, the distortion, which oscillates, increases in amplitude like R^{-4}. On the basis of these results, Naudé & Ellis (1961) analysed theoretically microjet formation in a non-hemispherical cavity in contact with a solid boundary, assuming that the liquid was inviscid and incompressible. Their theory starts from the linearized perturbation theory of Plesset & Mitchell (1955), and takes the second-order effects

into account to improve the solution when perturbation to the hemispherical shape becomes fairly large. Their theoretical results are in good agreement with their experiment on the collapse of a cavity generated by electric sparks.

In order to study the mechanism of cavitation damage, a number of experiments on the collapse of bubbles generated by electric sparks have been performed by many investigators (Shutler & Mesler 1965; Benjamin & Ellis 1966; Hammitt *et al.* 1970; Timm & Hammitt 1971; Popoviciu 1972; Anton & Popoviciu 1972; Smith & Mesler 1972). Each of their photographic studies shows that the collapse of a bubble near a solid wall, in translatory motion or in a pressure gradient, as in a venturi, is asymmetric; in particular a bubble collapsing in contact with a solid wall forms a liquid jet against the wall. But the interpretation of the mechanism of cavitation damage differs from one investigator to another, because it is possible that cavitation damage may be caused by the jet or by the high pressures developed near a bubble.

The behaviour of a bubble collapsing in the vicinity of a solid wall has been studied theoretically by Rattray (1951) and by Shima (1968).

The problem of the behaviour of a moving gas bubble in a flow field with a pressure gradient has been analysed by Yeh & Yang (1968). Their analyses, in which they assumed an incompressible and inviscid liquid, are based on perturbation theory or a polynomial expansion, therefore they become invalid as the deformation of the bubble increases.

From the viewpoint of mathematical analysis, the problem of non-spherical bubble collapse is fairly nonlinear and very complex, so that a worker cannot avoid using a numerical calculation method or an approximate treatment.

Plesset and Chapman studied the numerical simulation of a bubble collapsing near a solid wall (Plesset & Chapman 1971) and of an initially non-spherical bubble collapsing in an infinite liquid (Chapman & Plesset 1972), assuming irrotational flow. Their numerical method was based on solving the finite-difference equation of the potential problem by the Liebmann iterative method.

Mitchell & Hammitt (1973) simulated various asymmetric bubble collapses in an incompressible viscous liquid using a modified marker-and-cell technique.

Both simulations are quite good but are not easy to use to investigate the behaviour of a bubble. From this point of view the variational method for the dynamics of non-spherical bubbles which Hsieh (1972) has proposed may be useful for the approximate analysis of asymmetric bubble collapse. Taking the surface tension into account, in the present study the variational method was applied to the analysis of the collapse of a non-hemispherical bubble attached to a solid wall. The effects of surface tension on the collapse of a non-spherical bubble are important, especially in the case of a low pressure difference, a small bubble or a liquid with high surface tension.

2. Analysis

Let us consider the case of an axially symmetric bubble which collapses while attached to a solid wall. The spherical co-ordinate system shown in figure 1 is set up for the formulation of the problem.

The following assumptions will be made.

(i) The liquid is incompressible and inviscid.

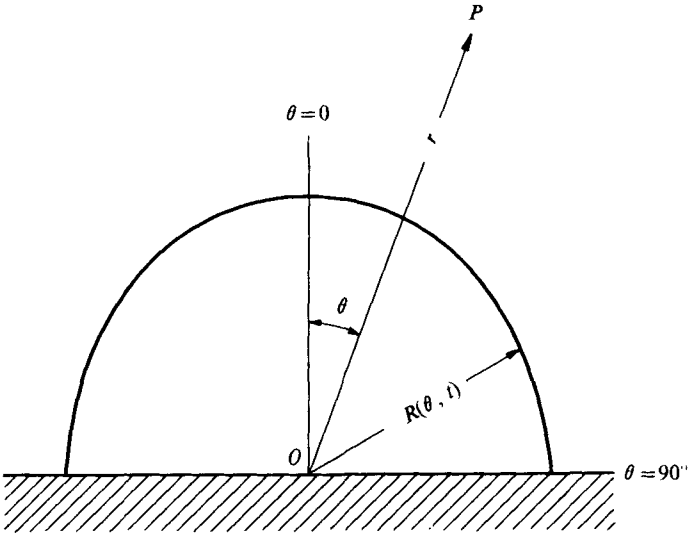

FIGURE 1. The spherical co-ordinate system.

(ii) The pressure inside the bubble is uniform. The ambient pressure is constant during the collapse.

(iii) The gas–liquid surface tension must be taken into account. The adhesion is negligible.

(iv) The effect of gravity is negligible.

(v) The effect of gas diffusion and the thermal effect are negligible.

We introduce assumption (i) to simplify the following analysis since we wish to study mainly the effect of surface tension on the behaviour of the bubble. In fact, the effect of liquid compressibility is less important except in the final stage of the collapse of a small gas bubble or a vapour bubble in which the vapour remains saturated. Also, the viscosity of the liquid may not be very important for a bubble collapsing in water under atmospheric pressure if the initial bubble radius is about 0·01 mm (Plesset & Chapman 1971).

Assumption (iii) is inconsistent with the real conditions in the immediate vicinity of the triple interface. However it appears to be difficult to obtain precisely the contact angle in the case of bubble motion, because it may change unsteadily. Therefore the gas–solid and the liquid–solid surface tensions are neglected in this paper, as in Naudé & Ellis (1961) and Chapman & Plesset (1972). Thus we take 90° as the contact angle.

The following analysis can be applied both to a gas bubble and to a vapour bubble. For the case of a vapour bubble, it is assumed that the interior of the bubble always remains in the saturated state corresponding to a given temperature. Then the problem reduces to solving Laplace's equation

$$\frac{1}{r^2}\frac{\partial}{\partial r}\left(r^2\frac{\partial \Phi}{\partial r}\right)+\frac{1}{r^2\sin\theta}\frac{\partial}{\partial \theta}\left(\sin\theta\frac{\partial \Phi}{\partial \theta}\right)=0, \tag{1}$$

where Φ is the velocity potential. The following boundary conditions must be satisfied:

$$\frac{\partial\Phi}{\partial r}-\frac{1}{R^2}\frac{\partial\Phi}{\partial\theta}\frac{\partial R}{\partial\theta}=\frac{\partial R}{\partial t} \quad \text{on} \quad r=R(\theta,t), \tag{2}$$

$$\frac{\partial\Phi}{\partial t}+\frac{1}{2}\left\{\left(\frac{\partial\Phi}{\partial r}\right)^2+\frac{1}{R^2}\left(\frac{\partial\Phi}{\partial\theta}\right)^2\right\}=\frac{1}{\rho}\left\{p_\infty-p_c+\sigma\left(\frac{1}{R_1}+\frac{1}{R_2}\right)\right\} \quad \text{on} \quad r=R(\theta,t), \tag{3}$$

where p_∞ is the pressure in the liquid at a great distance from the bubble, p_c the pressure inside the bubble, ρ the liquid density, σ the gas–liquid surface tension and R_1 and R_2 the principal radii of curvature of the bubble surface. The mean curvature is

$$\frac{1}{R_1}+\frac{1}{R_2}=\frac{R-R_\theta\cot\theta}{R[R^2+R_\theta^2]^{\frac{1}{2}}}+\frac{R^2+2R_\theta^2-RR_{\theta\theta}}{[R^2+R_\theta^2]^{\frac{3}{2}}}, \tag{4}$$

where $$R_\theta\equiv\partial R/\partial\theta, \quad R_{\theta\theta}\equiv\partial^2R/\partial\theta^2.$$

The remaining boundary conditions are

$$r^{-1}\partial\Phi/\partial\theta=0 \quad \text{on} \quad \theta=\tfrac{1}{2}\pi, \tag{5}$$

$$\Phi\to0 \quad \text{as} \quad r\to\infty. \tag{6}$$

As the initial conditions, the initial bubble shape $R(\theta,0)$ is given, and $\partial R/\partial t=0$ is chosen at $t=0$.

The problem governed by (1)–(6) can be shown to be equivalent to a variational problem: the solution of the above boundary-value problem is given by an extremum of the functional

$$J=2\pi\int_{t_1}^{t_2}dt\int_0^{\frac{1}{2}\pi}\sin\theta\,d\theta\left[-\frac{p_c-p_\infty}{3}R^3+\sigma R(R^2+R_\theta^2)^{\frac{1}{2}}+\int_{R(\theta,t)}^{\infty}\rho\left(\Phi_t+\tfrac{1}{2}\Phi_r^2+\frac{1}{2r^2}\Phi_\theta^2\right)r^2\,dr\right]. \tag{7}$$

This can be proved as follows. The first variation gives

$$\delta J=2\pi\int_{t_1}^{t_2}dt\left[\int_0^{\frac{1}{2}\pi}\sin\theta\,d\theta\int_{R(\theta,t)}^{\infty}\rho\left(\delta\Phi_t+\Phi_r\,\delta\Phi_r+\frac{1}{r^2}\Phi_\theta\,\delta\Phi_\theta\right)r^2\,dr+\int_0^{\frac{1}{2}\pi}\sin\theta\,d\theta\left\{-\rho\left(\Phi_t+\tfrac{1}{2}\Phi_r^2+\frac{1}{2r^2}\Phi_\theta^2\right)R^2\delta R-(p_c-p_\infty)R^2\delta R+\frac{\sigma[(2R^2+R_\theta^2)\,\delta R+RR_\theta\,\delta R_\theta]}{(R^2+R_\theta^2)^{\frac{1}{2}}}\right\}\right].$$

Then, after integration by parts, we have

$$\delta J=2\pi\int_{t_1}^{t_2}dt\left[-\int_0^{\frac{1}{2}\pi}\sin\theta\,d\theta\int_{R(\theta,t)}^{\infty}r^2\,dr\,\rho\left\{\frac{1}{r^2}(r^2\Phi_r)_r+\frac{1}{r^2\sin\theta}(\sin\theta\Phi_\theta)_\theta\right\}\delta\Phi+\int_0^{\frac{1}{2}\pi}\sin\theta\,d\theta\,\rho R^2\left(R_t-\Phi_r+\frac{R_\theta}{R^2}\Phi_\theta\right)_{r=R}\delta\Phi-\int_0^{\frac{1}{2}\pi}\sin\theta\,d\theta\,\rho R^2\left\{\Phi_t+\tfrac{1}{2}\Phi_r^2+\frac{1}{2R^2}\Phi_\theta^2+\frac{p_c-p_\infty}{\rho}-\frac{\sigma}{\rho}\left(\frac{R-R_\theta\cot\theta}{R(R^2+R_\theta^2)^{\frac{1}{2}}}+\frac{R^2+2R_\theta^2-RR_{\theta\theta}}{(R^2+R_\theta^2)^{\frac{3}{2}}}\right)\right\}_{r=R}\delta R+\int_{R(\frac{1}{2}\pi,t)}^{\infty}dr\,\rho(\Phi_\theta\,\delta\Phi)_{\theta=\frac{1}{2}\pi}+\sigma\left(\frac{RR_\theta\,\delta R}{(R^2+R_\theta^2)^{\frac{1}{2}}}\right)_{\theta=\frac{1}{2}\pi}\Bigg], \tag{8}$$

where we have used the boundary condition $\Phi \to 0$ at $r \to \infty$. Since the variations $\delta\Phi$ and δR are arbitrary, the conditions for obtaining an extremum of J lead to (1)–(6).

The last term in (8) should be determined from the contact angle with the solid wall. In this case, from assumption (iii) the contact angle is $\frac{1}{2}\pi$, so that $R_\theta = 0$ at $\theta = \frac{1}{2}\pi$.

Taking the boundary conditions (5) and (6) into consideration, we chose the set of trial functions as

$$\Phi(r,\theta,t) = \frac{\phi_0(t)}{r} + \sum_{n=1}^{N} \frac{\phi_{2n}(t)}{r^{2n+1}} P_{2n}(\cos\theta) \tag{9}$$

and

$$R(\theta,t) = R_0(t) + \sum_{n=1}^{N} R_{2n}(t)\, P_{2n}(\cos\theta), \tag{10}$$

where ϕ_0, ϕ_{2n}, R_0 and R_{2n} are time-dependent coefficients of the expansion and the $P_{2n}(\cos\theta)$ are Legendre polynomials.

The variations of Φ and R are

$$\delta\Phi = \frac{\delta\phi_0(t)}{r} + \sum_{k=1}^{N} \frac{\delta\phi_{2k}(t)}{r^{2k+1}} P_{2k}(\cos\theta) \tag{11}$$

and

$$\delta R = \delta R_0(t) + \sum_{k=1}^{N} \delta R_{2k}(t)\, P_{2k}(\cos\theta). \tag{12}$$

Since the trial function (9) satisfies the Laplace equation (1), by substituting (9)–(12) in (8) we obtain

$$\delta J = 2\pi \int_{t_1}^{t_2} dt \sum_{k=0}^{N} \int_0^{\frac{1}{2}\pi} \sin\theta\, d\theta\, \rho R^2 \left[\left\{ R_t - \Phi_r + \frac{R_\theta \Phi_\theta}{R^2} \right\} \frac{P_{2k}(\cos\theta)}{R^{2k+1}}\, \delta\phi_{2k} \right.$$
$$\left. - \left\{ \Phi_t + \tfrac{1}{2}\Phi_r^2 + \frac{1}{2R^2}\Phi_\theta^2 + \frac{p_c - p_\infty}{\rho} - \frac{\sigma}{\rho}\left(\frac{1}{R_1} + \frac{1}{R_2}\right) \right\} P_{2k}(\cos\theta)\, \delta R_{2k} \right]. \tag{13}$$

Since $\delta\phi_{2k}$ and δR_{2k} are arbitrary, the extremal conditions are

$$\int_0^{\frac{1}{2}\pi} \left\{ R_t - \Phi_r + \frac{R_\theta \Phi_\theta}{R^2} \right\} \frac{P_{2k}(\cos\theta)}{R^{2k+1}} \sin\theta\, d\theta = 0, \tag{14}$$

$$\int_0^{\frac{1}{2}\pi} \left\{ \Phi_t + \tfrac{1}{2}\Phi_r^2 + \frac{1}{2R^2}\Phi_\theta^2 + \frac{p_c - p_\infty}{\rho} - \frac{\sigma}{\rho}\left(\frac{1}{R_1} + \frac{1}{R_2}\right) \right\} R^2 P_{2k} \sin\theta\, d\theta = 0, \tag{15}$$

where $k = 0, 1, \ldots, N$. In order to solve (14) and (15) for ϕ_{2n} and R_{2n}, it is convenient to express these equations in the following matrix form:

$$\mathbf{M\Phi} + \mathbf{F\dot{R}} = 0, \quad \mathbf{F}^{\mathrm{T}}\dot{\mathbf{\Phi}} + \mathbf{S} = 0, \tag{16), (17}$$

where

$$\mathbf{\Phi} = \{\phi_0, \phi_2, \ldots, \phi_{2N}\}^{\mathrm{T}}, \quad \mathbf{R} = \{R_0, R_2, \ldots, R_{2N}\}^{\mathrm{T}}, \tag{18), (19}$$

$$M_{kn} = \int_0^{\frac{1}{2}\pi} \frac{P_{2k}}{R^{2n+2k+1}} \left\{ (2n+1)\, P_{2n} + \frac{R_\theta}{R}\frac{dP_{2n}}{d\theta} \right\} \sin\theta\, d\theta, \tag{20}$$

$$F_{kn} = \int_0^{\frac{1}{2}\pi} \frac{P_{2k} P_{2n}}{R^{2k-1}} \sin\theta\, d\theta, \tag{21}$$

$$S_k = \int_0^{\frac{1}{2}\pi} \left[\frac{1}{2} \left(\frac{\phi_0}{R} + \sum_{n=1}^{N} \frac{2n+1}{R^{2n+1}} \phi_{2n} P_{2n} \right)^2 + \frac{1}{2} \left(\sum_{n=1}^{N} \frac{\phi_{2n}}{R^{2n+1}} \frac{dP_{2n}}{d\theta} \right)^2 \right.$$
$$\left. - \frac{1}{\rho} \left\{ p_\infty - p_c + \sigma \left(\frac{1}{R_1} + \frac{1}{R_2} \right) \right\} R^2 \right] P_{2k} \sin\theta\, d\theta. \tag{22}$$

From (16), we obtain

$$\boldsymbol{\Phi} = -\mathbf{M}^{-1}\mathbf{F}\dot{\mathbf{R}}. \tag{23}$$

By substituting (23) in (17), an equation governing the motion of the bubble can be obtained:

$$\ddot{\mathbf{R}} = \mathbf{F}^{-1}[(\dot{\mathbf{M}}\mathbf{M}^{-1}\mathbf{F} - \dot{\mathbf{F}})\dot{\mathbf{R}} + \mathbf{M}(\mathbf{F}^{\mathrm{T}})^{-1}\mathbf{S}], \tag{24}$$

where

$$\dot{M}_{kn} = -\int_0^{\frac{1}{2}\pi} \frac{P_{2k}}{R^{2n+2k+2}}\left[(2n+1)(2n+2k+1)\dot{R}P_{2n} + (2n+2k+2)\frac{\dot{R}R_\theta}{R}\frac{dP_{2n}}{d\theta} - \dot{R}_\theta\frac{dP_{2n}}{d\theta}\right] \times \sin\theta\, d\theta, \tag{25}$$

$$\dot{F}_{kn} = -(2k-1)\int_0^{\frac{1}{2}\pi} \frac{P_{2k}P_{2n}}{R^{2k}}\dot{R}\sin\theta\, d\theta. \tag{26}$$

If the initial conditions on $\mathbf{R}$ and $\dot{\mathbf{R}}$ at $t = 0$ are given, the ordinary simultaneous differential equation (24) can be solved numerically.

Assuming that the gas inside a gas bubble is ideal and undergoes an adiabatic process during the growth or collapse of the bubble, the pressure inside the bubble will be

$$p_c = p_{G0}[V_c(0)/V_c(t)]^\gamma, \tag{27}$$

where p_{G0} is the initial gas pressure, γ is the ratio of the specific heats of the gas, and $V_c(t)$ is the bubble volume at time t:

$$V_c(t) = \tfrac{2}{3}\pi\int_0^{\frac{1}{2}\pi} R^3(\theta, t)\sin\theta\, d\theta. \tag{28}$$

On the other hand, for the case of a vapour bubble it follows that

$$p_c = \text{constant}. \tag{27'}$$

The pressure distribution in the liquid can be obtained by substituting (9) in Bernoulli's equation:

$$p(r,t) = p_\infty - \rho\left\{\frac{\partial\Phi}{\partial t} + \frac{1}{2}\left(\frac{\partial\Phi}{\partial r}\right)^2 + \frac{1}{2r^2}\left(\frac{\partial\Phi}{\partial\theta}\right)^2\right\}. \tag{29}$$

Similarly, the pressure on the bubble surface can be obtained by using the relation

$$p_R = p_c - \sigma(R_1^{-1} + R_2^{-1}). \tag{30}$$

3. Results of the calculations

All physical quantities involving length, velocity, acceleration, time, pressure and surface tension may be non-dimensionalized by dividing by

$$R_0(0), \quad \left(\frac{p_\infty}{\rho}\right)^{\frac{1}{2}}, \quad \frac{1}{R_0(0)}\frac{p_\infty}{\rho}, \quad \frac{R_0(0)}{(p_\infty/\rho)^{\frac{1}{2}}}, \quad p_\infty, \quad p_\infty R_0(0)$$

respectively. We performed the calculations with all equations in dimensionless form. Equation (24) was numerically integrated by the Runge–Kutta–Gill method on the digital computer NEAC-2200-MODEL-700 in the Computer Center, Tōhoku University.

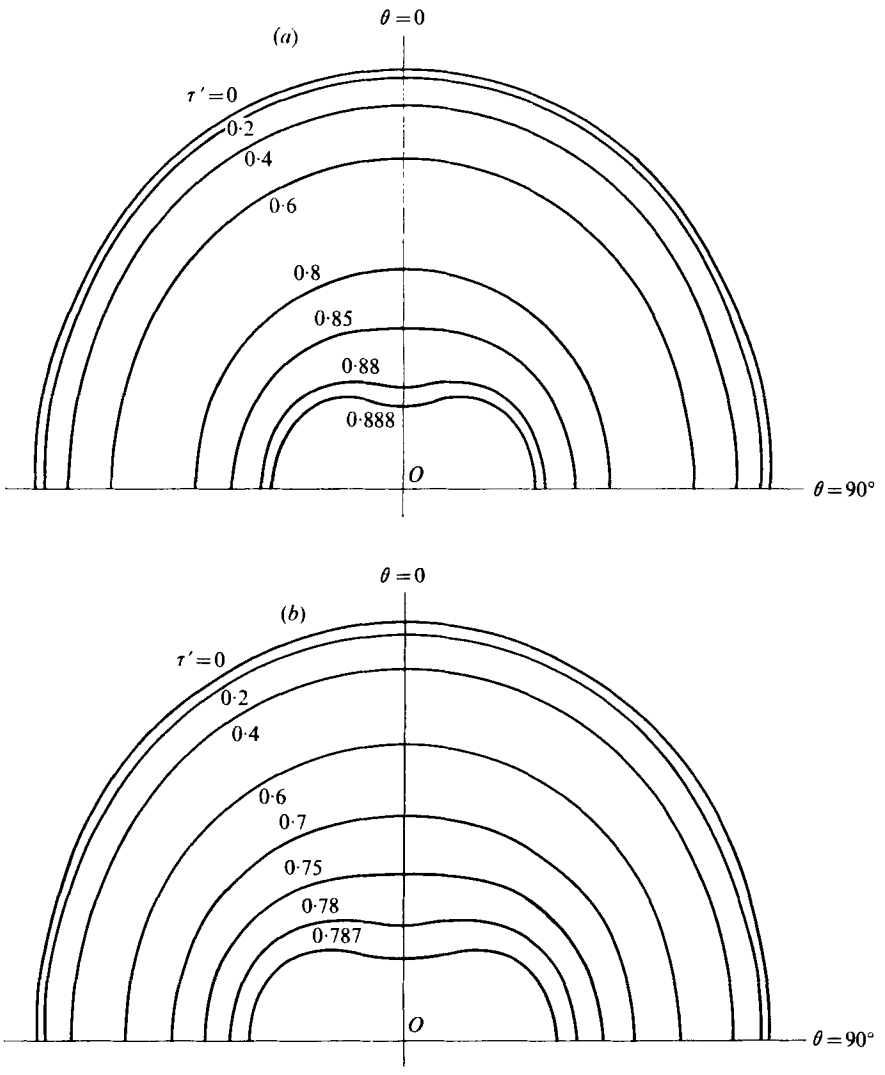

FIGURE 2. Bubble surface profiles for case A; $\tau' \equiv (t/R_0(0))\,[(p_\infty - p_c)/\rho]^{\frac{1}{2}}$. (*a*) Without surface tension; $T \equiv \sigma/R_0(0)\,(p_\infty - p_c) = 0$. (*b*) With surface tension; $T = 0{\cdot}1$.

We calculated two cases of the collapse of an initially non-hemispherical bubble attached to a solid wall. The first of these (case A) had a prolate initial bubble shape with radius

$$R(\theta, 0) = 1 + 0{\cdot}1P_2(\cos\theta). \tag{31}$$

The other (case B) had an oblate initial shape with radius

$$R(\theta, 0) = 1 - 0{\cdot}1P_2(\cos\theta). \tag{32}$$

The liquid was assumed to be initially static in both cases, so that $\dot{R}(\theta, 0) = 0$ was chosen. The calculations were carried out keeping 8 terms (up to $N = 7$) in (9) and (10); that is, 8 equations for $R_0, R_2, \ldots, R_{14}$ were involved in (24). Although we increased the number of equations, we expected hardly any improvement in the solution.

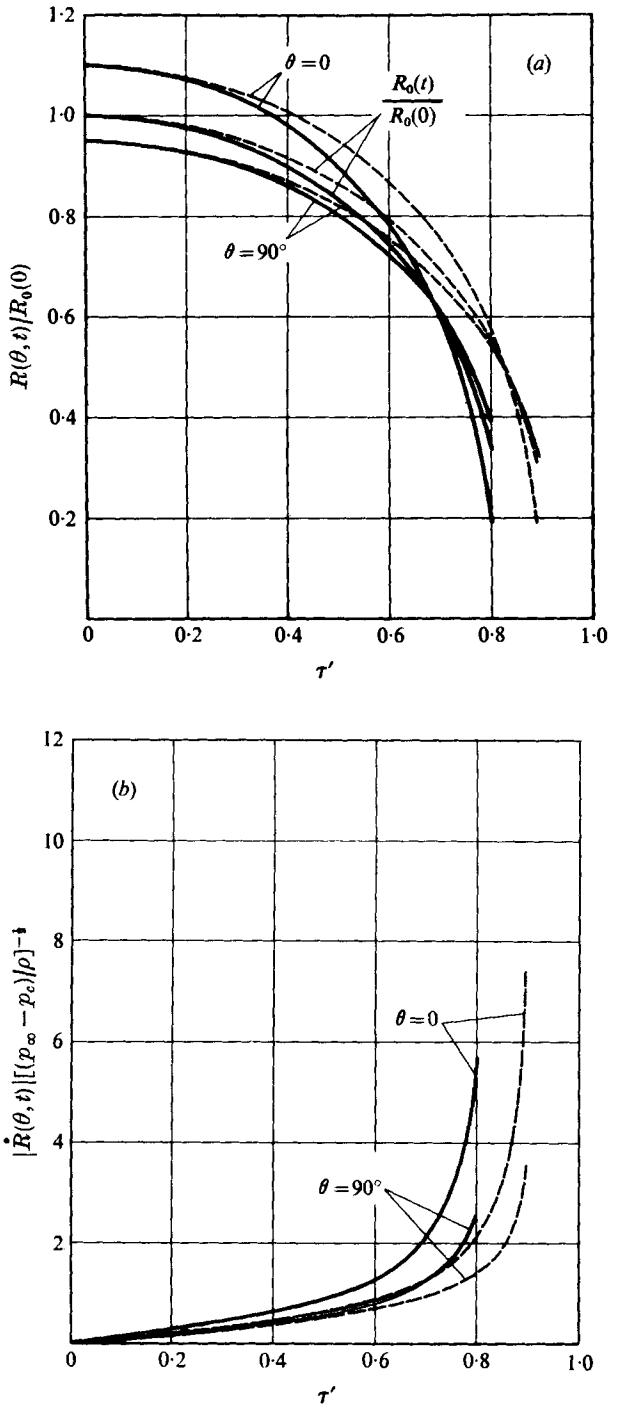

FIGURE 3. (*a*) Radii of bubble surface on the axis of symmetry and on the solid wall and the mean radius $R_0(t)/R_0(0)$ and (*b*) velocities of the bubble surface on the axis of symmetry and on the solid wall all as functions of time for case *A*. ——, $T = 0{\cdot}1$; – – –, $T = 0$.

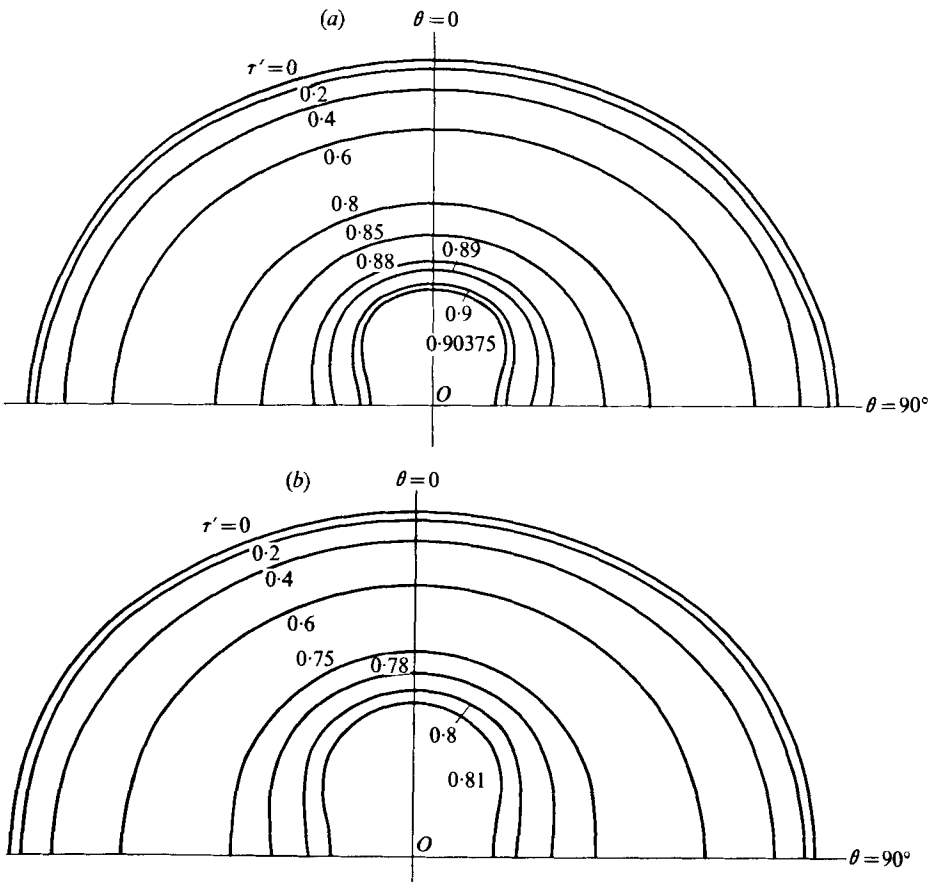

FIGURE 4. Bubble surface profiles for case B (*a*) without surface tension ($T = 0$) and (*b*) with surface tension ($T = 0{\cdot}1$).

The collapse of a non-hemispherical bubble with constant internal pressure

Figures 2–7 are concerned with the behaviour of a bubble with constant internal pressure collapsing when attached to a solid wall. The collapse is brought about by the difference between the ambient pressure p_∞ and the internal pressure p_c. This pressure difference $p_\infty - p_c$ is also taken to be constant. If velocities and time are non-dimensionalized by $[(p_\infty - p_c)/\rho]^{\frac{1}{2}}$ and $R_0(0)\ [(p_\infty - p_c)/\rho]^{-\frac{1}{2}}$ respectively, the characteristics of the collapse under various pressure differences will be scaled to give similar results.

It is obvious from the study of Numachi (1958) that comparatively small bubbles play an important part in cavitation damage. It should be remembered that the surface tension of the liquid has an important effect on the behaviour, in particular the collapse of small bubbles in such cases. Now consider a bubble in water under atmospheric pressure. In this case, for $R_0 = 0{\cdot}01$ mm, $p_\infty - p_c \simeq 10^6$ dynes/cm^2 and $\sigma = 73$ dynes/cm (at 20° C) the dimensionless surface tension $T = \sigma/R_0(p_\infty - p_c)$ is 0·073. In this work, therefore, we calculated the two cases where the dimensionless surface tension is 0·1 and 0 in order to study the effect of the surface tension. Figures 2(*a*) and (*b*) show the time history of the bubble shape for case A without and with

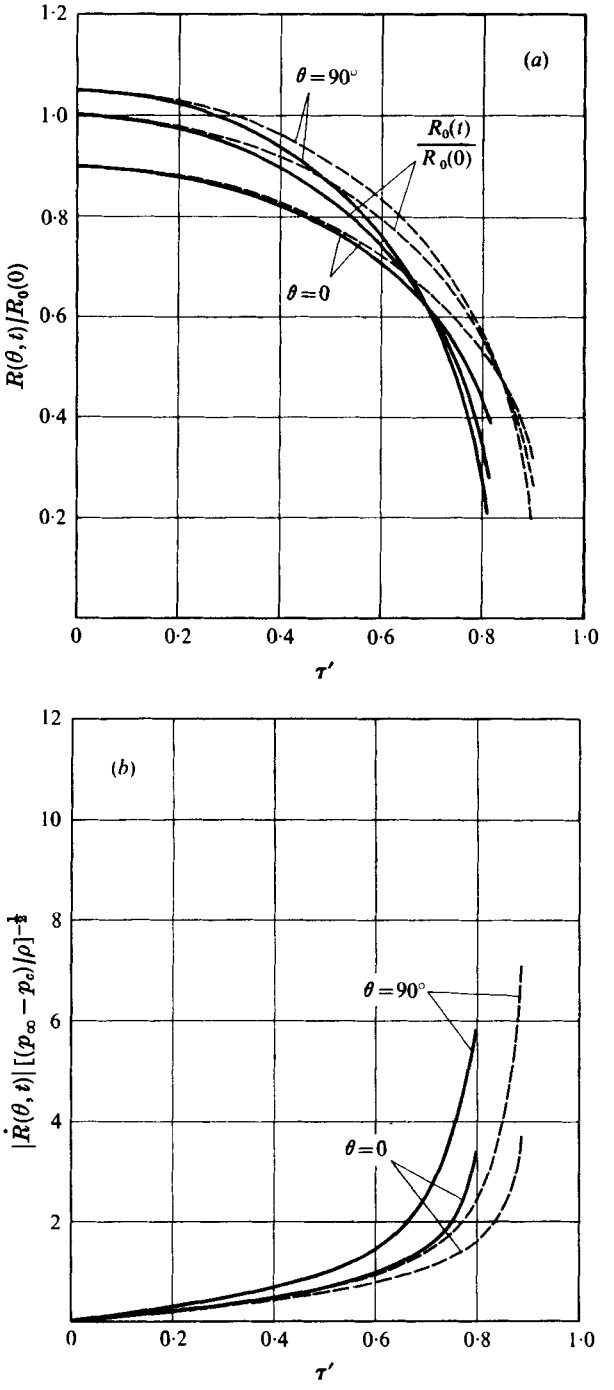

FIGURE 5. (*a*) Radii of the bubble surface on the axis of summetry and on the solid wall and the mean radius $R_0(t)/R_0(0)$ and (*b*) velocities of the bubble surface on the axis of symmetry and on the solid wall all as functions of time for case *B*. ——, $T = 0{\cdot}1$; – – –, $T = 0$.

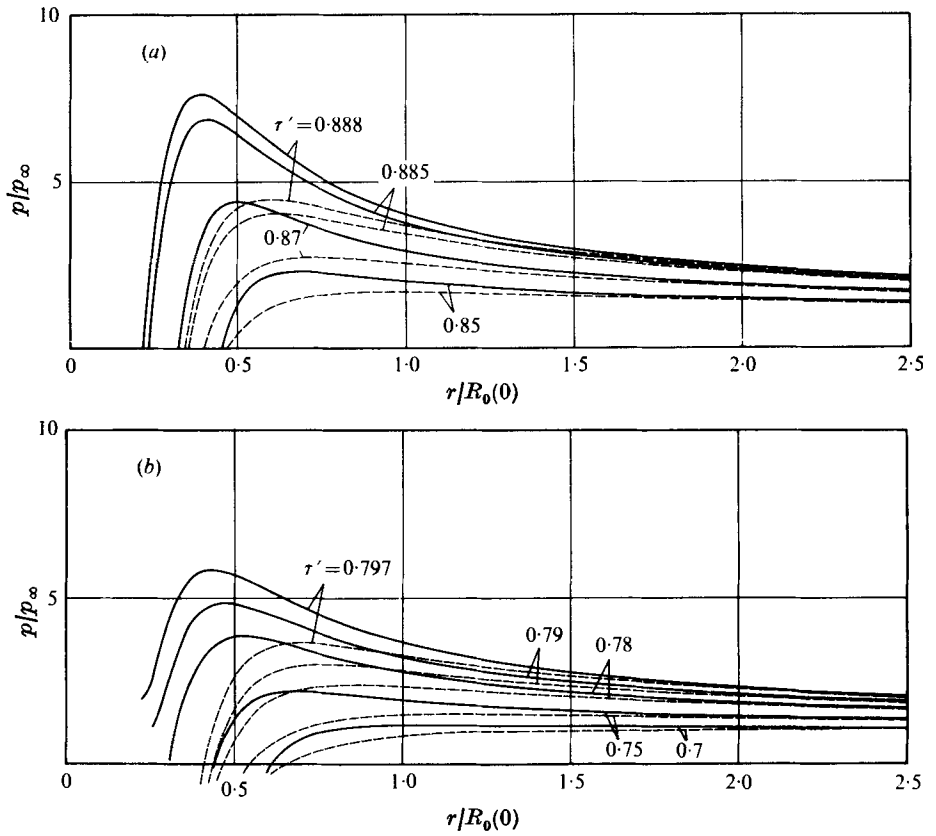

FIGURE 6. Pressure distributions along the axis of symmetry and along the solid wall at several times during collapse for case A; (a) without surface tension ($T = 0$) and (b) with surface tension ($T = 0{\cdot}1$). ——, $\theta = 0$; – – –, $\theta = 90°$.

surface tension respectively. In this case, since the velocity on the bubble surface is greatest at the pole, the bubble shape changes from the prolate initial shape to an oblate one, and eventually this deformation will cause the formation of a jet on the axis of symmetry. A comparison of figure 2(a) with figure 2(b) shows that surface tension increases the deformation of the bubble in the final stages of collapse. On the concave part of the bubble surface, the liquid pressure outside the bubble is higher than that inside because of the negative curvature. Thus the deformation of the bubble tends to increase. The radii and velocities of the bubble surface on the axis of symmetry $\theta = 0$ and on the solid wall $\theta = \frac{1}{2}\pi$ in case A are shown as a function of time in figures 3(a) and (b) respectively. In figure 3(a) the mean radius $R_0(t)/R_0(0)$ as a function of time is also shown. These figures clearly indicate that surface tension accelerates the collapse of a bubble. But surface tension may not necessarily increase the final velocity of the jet when it strikes the wall.

At the end of the calculation, the velocity of the bubble surface on the axis of symmetry reached about $60 \sim 70$ m/s in water under a pressure difference of one atmosphere (1·013 bar).

For case B, figures 4 and 5 show results similar to those for case A. In this case, the velocity on the bubble surface is a maximum on the solid wall, and the oblate

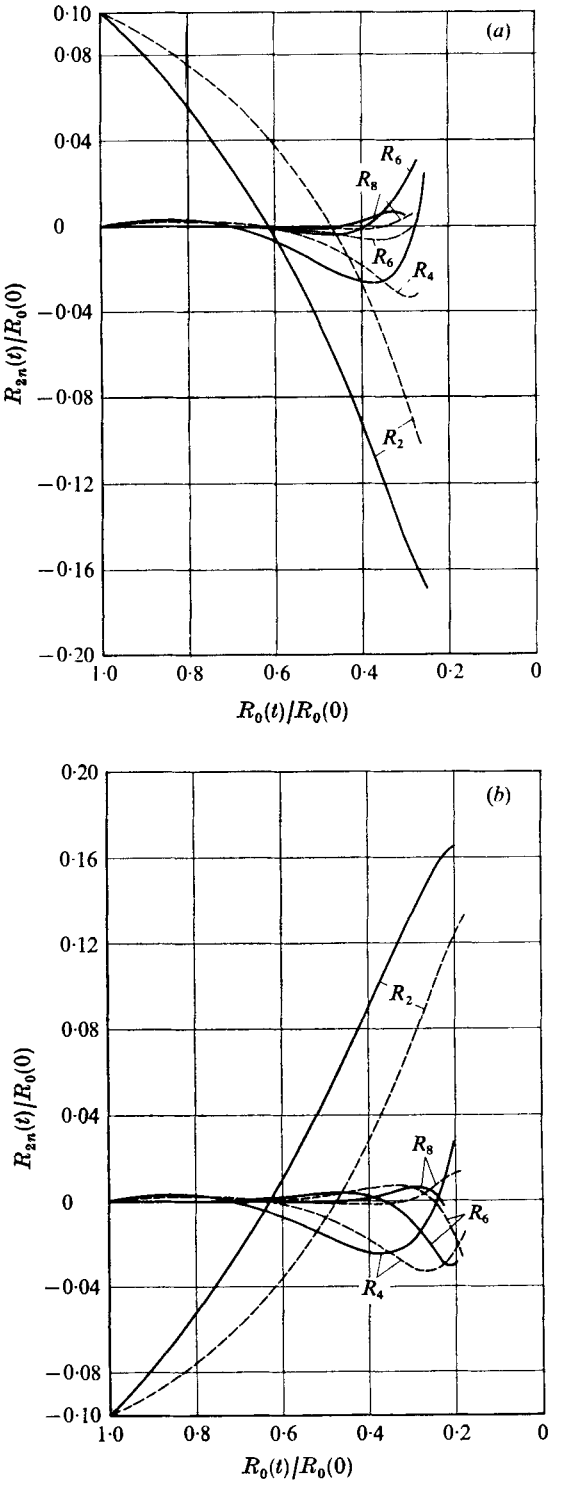

FIGURE 7. Coefficients in expansion of bubble radius for (*a*) case *A* and (*b*) case *B*. ——, $T = 0{\cdot}1$; – – –, $T = 0$.

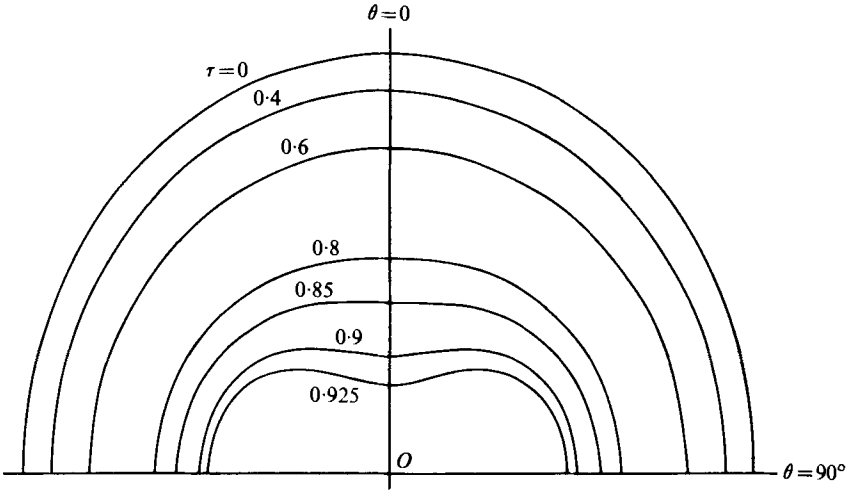

FIGURE 8. Bubble surface profiles at several times during collapse with an initial gas pressure $p_{G0}/p_\infty = 0{\cdot}2$. $\gamma = 1{\cdot}4$, $T = 0{\cdot}1$.

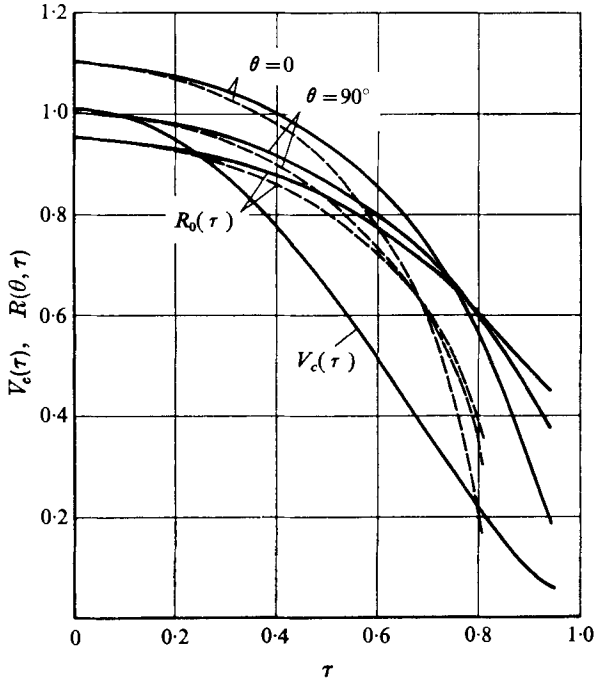

FIGURE 9. Radii of the bubble surface on the axis of symmetry and on the solid wall, the mean radius $R_0(\tau)$ and the bubble volume $V_c(\tau)$ as functions of time τ. $\gamma = 1{\cdot}4$, $T = 0{\cdot}1$. ——, $p_{G0}/p_\infty = 0{\cdot}2$; – – –, $p_{G0}/p_\infty = 0$.

bubble shape is transformed into a bell shape. In potential flow, the collapse of a nearly hemispherical bubble attached to a solid wall is the same problem as the collapse of a nearly spherical bubble with a plane of symmetry in an infinite liquid, because the boundary condition at the plane of symmetry in the nearly spherical case, i.e. no flow across that plane, is the same as that at the solid wall in the nearly hemispherical

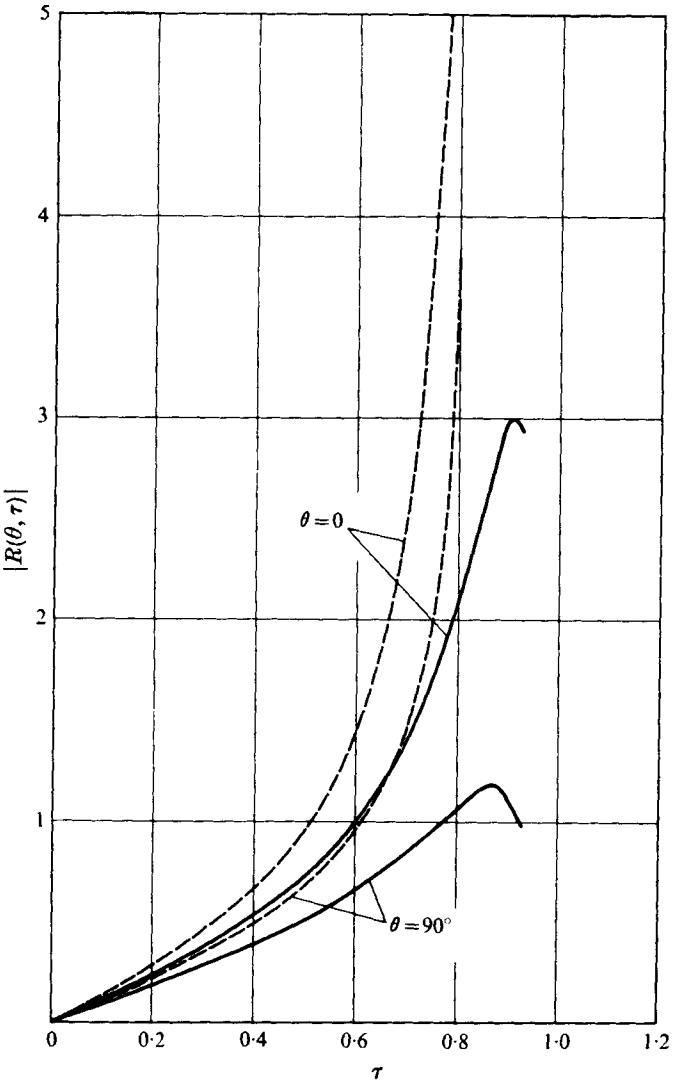

FIGURE 10. Velocities of the bubble surface on the axis of symmetry and on the solid wall as functions of time. $\gamma = 1{\cdot}4$, $T = 0{\cdot}1$. Curves as in figure 9.

case. Moreover, there is no adhesion to the solid wall in this problem, so that nothing prevents the bubble surface on the solid wall from having a maximum velocity as well as the pole in case A.

Figures 6(a) and (b) show the pressure distributions along the axis of symmetry $\theta = 0$ and along the solid wall $\theta = \frac{1}{2}\pi$ at several times during the collapse in case A without and with surface tension respectively. For the calculation of the relative pressure p/p_∞ in the liquid, the pressure p_c inside the bubble is taken to be zero. In the final stages of collapse, the pressure attains a peak value near the bubble surface, and decreases rapidly to p_∞ with radial distance from the bubble surface.

We find here that the pressure development along the solid wall is rather slower than that along the axis of symmetry. It is to be noted that the pressure on the bubble

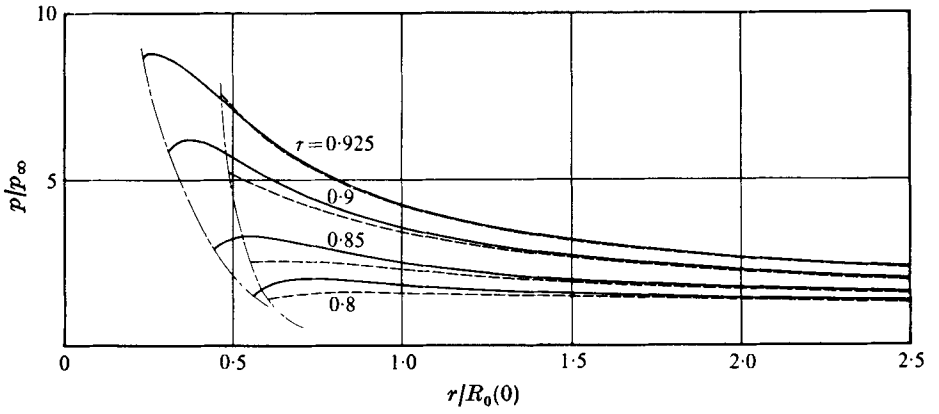

FIGURE 11. Pressure distributions along the axis of symmetry and along the solid wall at several times during the collapse. $p_{G0}/p_\infty = 0{\cdot}2$, $T = 0{\cdot}1$. ——, $\theta = 0$; – – –, $\theta = 90°$.

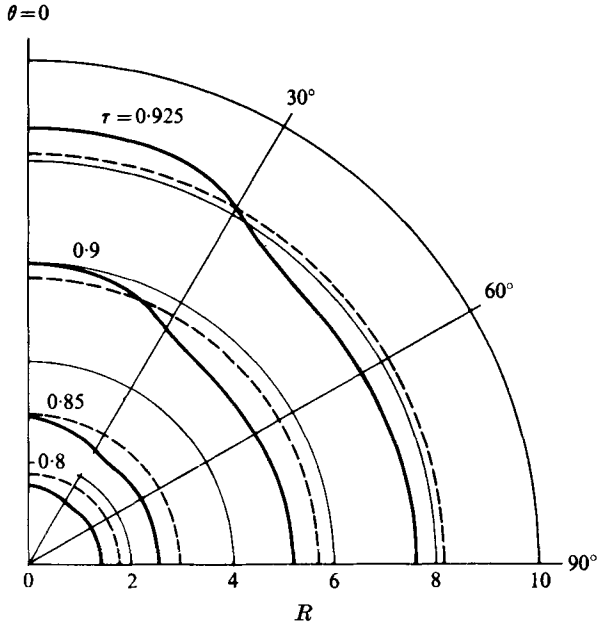

FIGURE 12. Pressure distributions on the bubble surface and gas pressures inside the bubble at several times. $p_{G0}/p_\infty = 0{\cdot}2$, $\gamma = 1{\cdot}4$, $T = 0{\cdot}1$. ——, p_R/p_∞; – – –, p_c/p_∞.

surface is not equal to zero in the collapse with surface tension, as shown in figure 6 (*b*). This fact can be seen from (30); that is, under this condition, the pressure on the convex part of the surface is negative because of the positive curvature, while that on the concave part is positive because of the negative curvature.

Figures 7 (*a*) and (*b*) show the coefficients $R_2(t)$, $R_4(t)$, $R_6(t)$ and $R_8(t)$ as a function of $R_0(t)$ for cases A and B respectively. The results obtained by taking surface tension into consideration and the results obtained without surface tension are shown in these figures. Of course, the latter results are in agreement with those calculated numerically by Chapman & Plesset (1972). Therefore it may be estimated that this variational

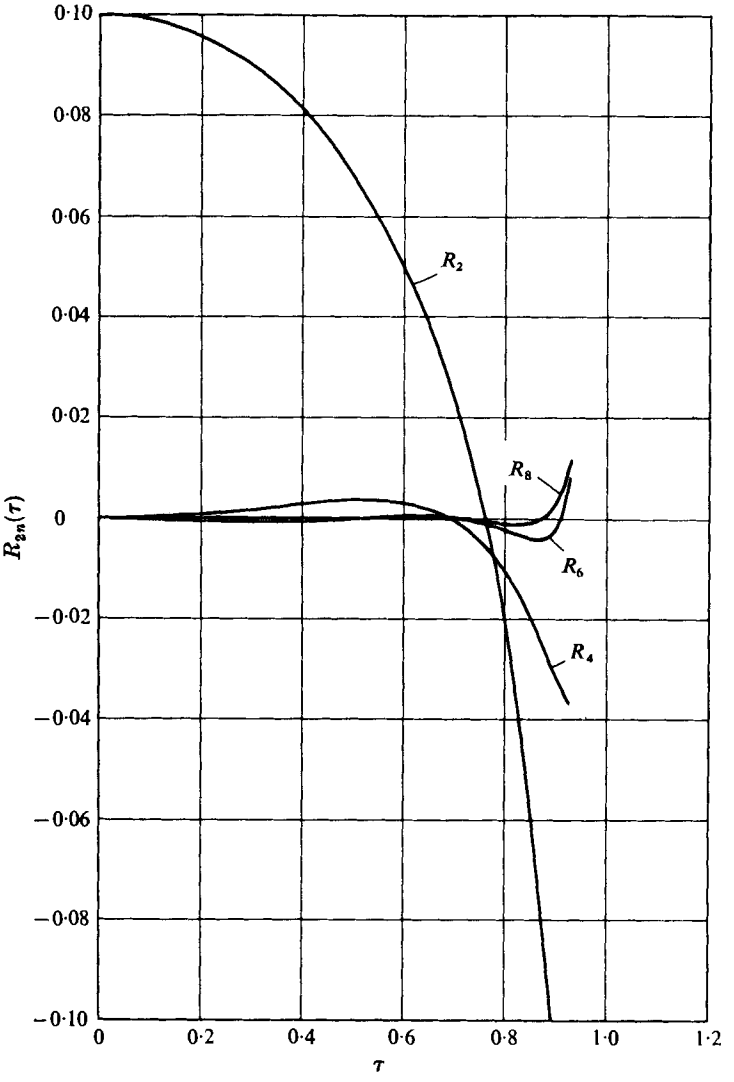

FIGURE 13. Coefficients in expansion of bubble radius as functions of time. $p_{G0}/p_\infty = 0{\cdot}2$, $\gamma = 1{\cdot}4$, $T = 0{\cdot}1$.

method gives about the same degree of accuracy as the finite-difference approximation of Chapman & Plesset.

Although the higher-order coefficients R_{2n} for $n \geqslant 2$ are zero at first, their amplitude increases with oscillation, because of nonlinear effects, and tends to diverge as the mean radius approaches zero. The rates of the divergence of $\dot{R}_{2n}$ and $\ddot{R}_{2n}$ are even greater. Because these terms interact in the nonlinear equations (24), their solutions become unstable, at which point the calculation was stopped.

The behaviour of a non-hemispheical bubble with internal pressure undergoing an adiabatic process

Figures 8–20 are concerned with the behaviour of a non-hemispherical bubble attached to a solid wall with internal gas pressure undergoing an adiabatic process. The value

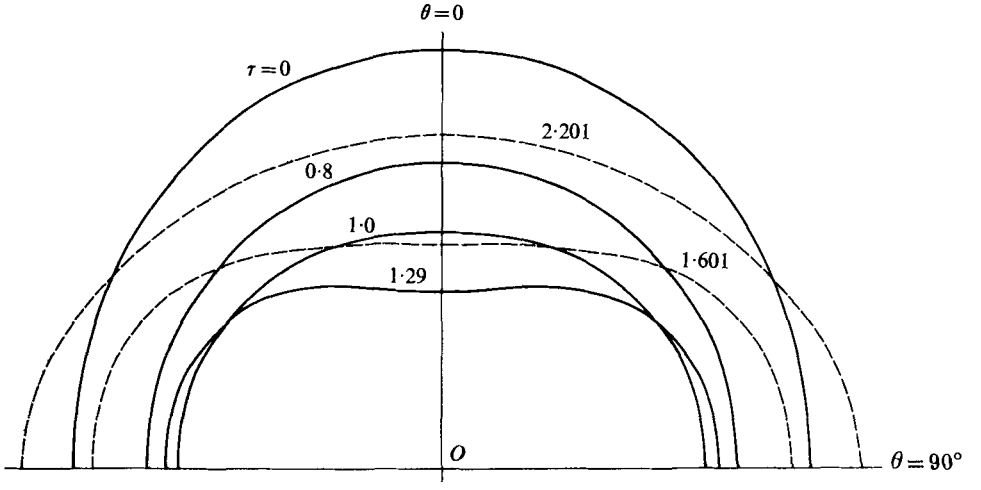

FIGURE 14. Bubble surface profiles at several times during the oscillation with an initial gas pressure $p_{G0}/p_\infty = 0{\cdot}5$ and with surface tension $T = 0{\cdot}1$; $\gamma = 1{\cdot}4$.

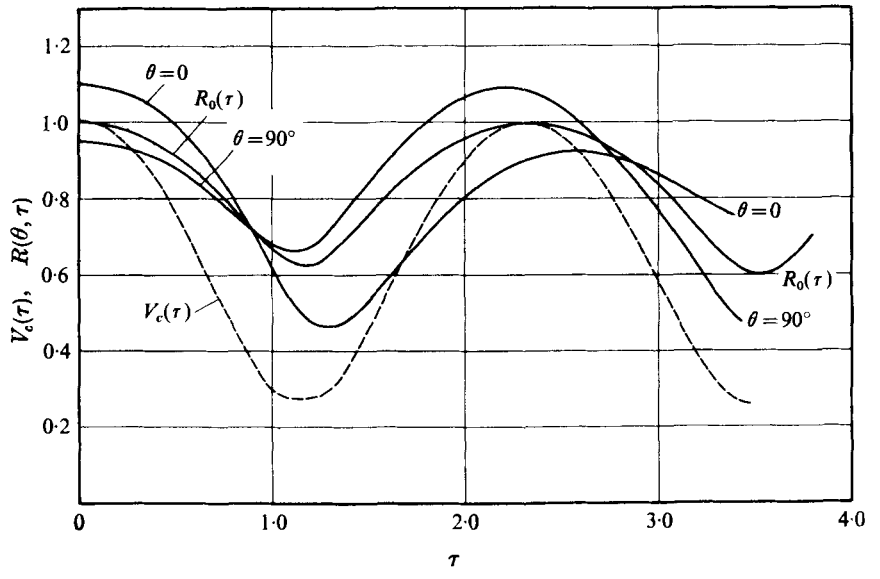

FIGURE 15. Radii of the bubble surface on the axis of symmetry and on the solid wall, the mean radius $R_0(\tau)$ and the bubble volume $V_c(\tau)$ as functions of time. $p_{G0}/p_\infty = 0{\cdot}5$, $\gamma = 1{\cdot}4$, $T = 0{\cdot}1$.

of γ was taken to be 1·4. The initial bubble shape of case A, given by (31), was used in this calculation.

The characteristics of the bubble collapse for an initial gas pressure $p_{G0}/p_\infty = 0{\cdot}2$ and a dimensionless surface tension $T(= \sigma/R_0(0)\,p_\infty) = 0{\cdot}1$ are shown in figures 8–12. Figure 8 shows the time history of the bubble shape for case A. Figure 9 shows the radii of the bubble surface on the axis of symmetry $\theta = 0$ and on the solid wall $\theta = \frac{1}{2}\pi$, the mean radius $R_0(t)$ and the bubble volume $V_0(\tau)$ as a function of time. Figure 10 shows the velocities of the bubble surface on the axis of symmetry and on the solid

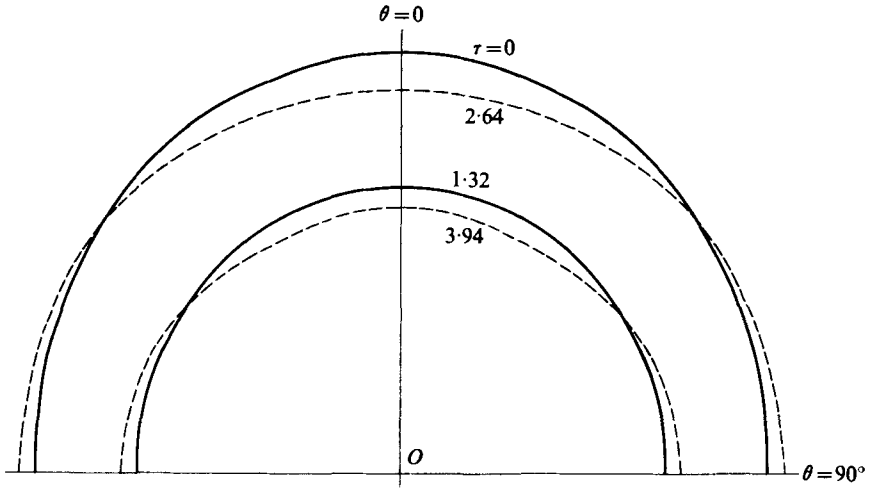

FIGURE 16. Bubble surface profiles at several times during the oscillation with an initial gas pressure $p_{G0}/p_\infty = 0{\cdot}5$ without surface tension ($T = 0$); $\gamma = 1{\cdot}4$.

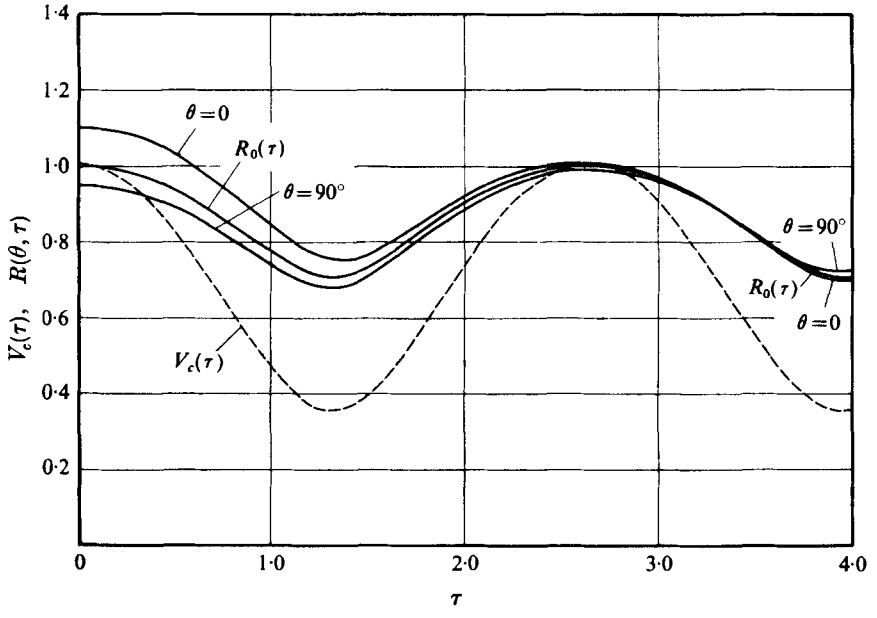

FIGURE 17. Radii of the bubble surface on the axis of symmetry and on the solid wall, the mean radius $R_0(\tau)$ and the bubble volume $V_c(\tau)$ as functions of time. $p_{G0}/p_\infty = 0{\cdot}5$, $\gamma = 1{\cdot}4$, $T = 0$.

wall as a function of time. In figures 9 and 10 respectively, the radii and velocities of the bubble surface for collapse with constant internal pressure, $p_{G0}/p_\infty = 0$, are also included. It is to be noted here that the cushioning effect of internal gas compression retards the collapse of a bubble, and eventually the bubble will rebound.

Figure 11 shows pressure distributions along the axis of symmetry and along the solid wall at different times during the collapse. In comparison with figure 6(*b*), we note that the pressure distribution along the solid wall is in close agreement with

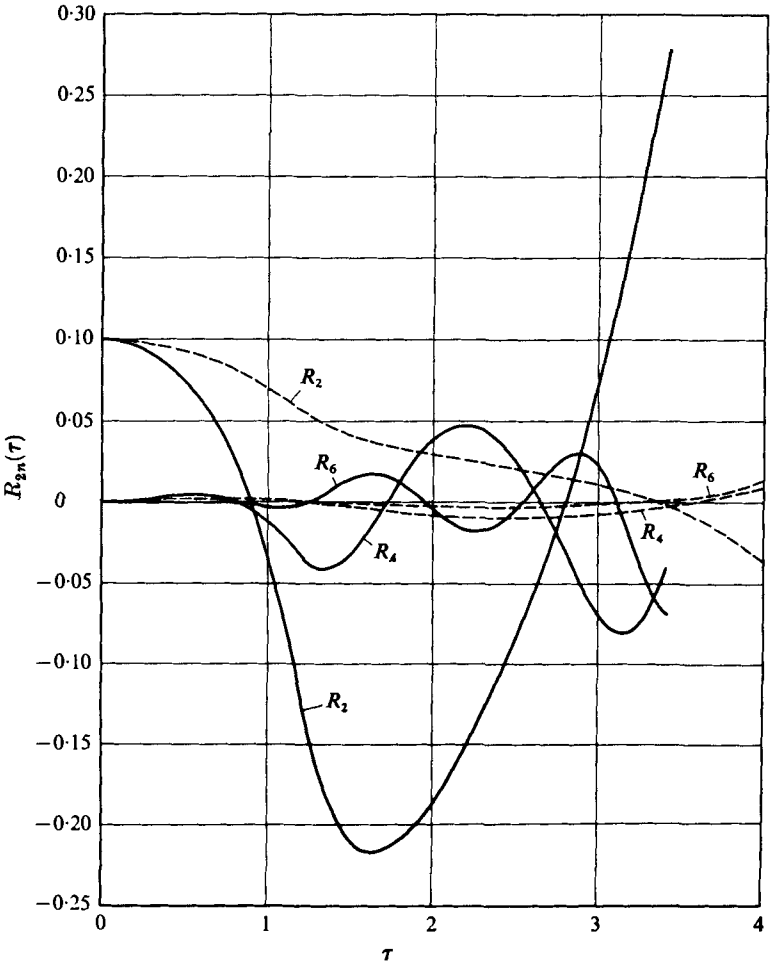

FIGURE 18. Coefficients in expansion of bubble radius as functions of time. $p_{G0}/p_\infty = 0{\cdot}5$, $\gamma = 1{\cdot}4$. ——, $T = 0{\cdot}1$; – – –, $T = 0$.

that along the axis of symmetry in the final stages of the collapse, and that the peak pressure in the liquid is higher than that for collapse with constant internal pressure. This may be explained by the fact that kinetic energy of the liquid is transformed into potential energy of the gas, i.e. kinetic energy of the liquid is given to the gas, and causes the gas pressure to rise.

Figure 12 shows the pressure distributions on the bubble surface calculated by using (30), and gas pressures inside the bubble calculated at different times during the collapse. The pressure near the pole in the final stage of the collapse was higher than the gas pressure because of the negative curvature of the bubble surface.

Figure 13 shows the coefficients R_2, R_4, R_6 and R_8 as a function of time.

Figures 14–20 are concerned with the behaviour of the bubble for an initial gas pressure $p_{G0}/p_\infty = 0{\cdot}5$ and a dimensionless surface tension $T = 0{\cdot}1$ or 0. The bubble shape history for $T = 0{\cdot}1$ is shown in figure 14. The radii of the bubble surface on the axis of symmetry $\theta = 0$ and on the solid wall $\theta = \frac{1}{2}\pi$, the mean radius $R_0(\tau)$ and the bubble volume $V_c(\tau)$ are shown in figure 15 as a function of time. The bubble undergoes

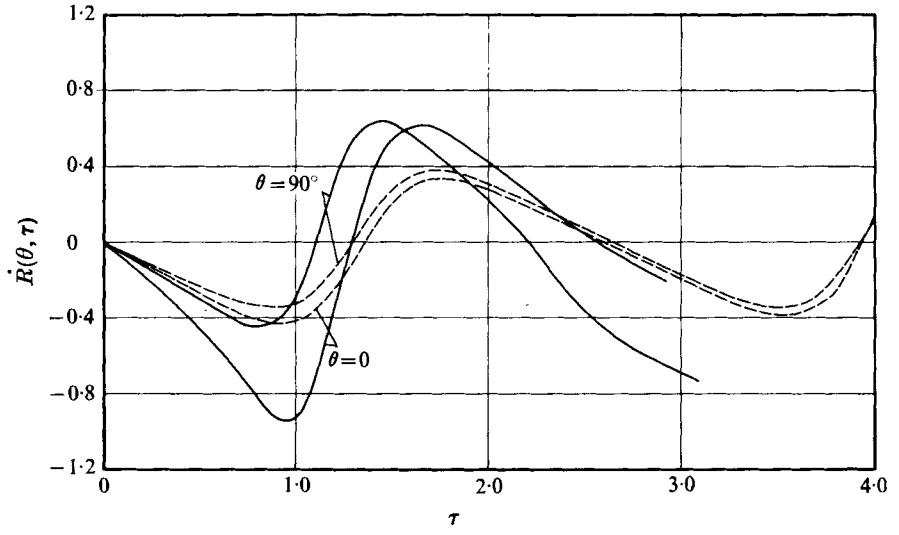

FIGURE 19. Velocities of the bubble surface on the axis of symmetry and on the solid wall as functions of time. $p_{G0}/p_\infty = 0{\cdot}5$, $\gamma = 1{\cdot}4$. ——, $T = 0{\cdot}1$; – – –, $T = 0$.

the volume pulsation associated with the second mode of shape oscillation. Figure 16 shows the bubble shape history in the case where the surface tension was not taken into consideration. Figure 17 shows the radii of the bubble surface at $\theta = 0$ and $\frac{1}{2}\pi$, the mean radius and the bubble volume for $T = 0$ as a function of time. In this case, the bubble tends to change from the initial prolate hemispheroid to the hemispherical shape during the oscillation, and undergoes only a volume pulsation.

Accordingly, it is to be noted that the shape oscillation is caused by surface tension. Figure 18 shows the variation of the coefficients R_2, R_4 and R_6 with time. By taking the surface tension into consideration, it can be seen that these coefficients oscillate with increasing amplitudes. If surface tension is neglected, R_2, whose initial value is 0·1, gradually decreases without oscillation, while R_4 and R_6, which are initially zero, grow only slightly.

Figure 19 shows the variation in the velocities of the bubble surface on the axis of symmetry $\theta = 0$ and on the solid wall $\theta = \frac{1}{2}\pi$ as a function of time. Figure 20 shows the variation of the pressure on the bubble surface at $\theta = 0$ and $\frac{1}{2}\pi$ and the internal gas pressure as a function of time. These figures show that the peak values of the velocities and pressures on the bubble surface in the case where the surface tension is taken into account are considerably higher than those without it. It may be presumed that the energy of the deforming motion caused by surface tension contributes to the increases in the velocity and pressure on the bubble surface.

Lastly, we should like to compare the variational method and the finite-difference method. The method used in our paper is the so-called direct variational technique, in which the solution is obtained approximately from the extremal condition for a functional after replacing the given problem with an equivalent problem. It is applied when the governing equations are difficult to solve or the solution of a given partial differential equation is not easy. For example, a problem which is governed by a partial differential equation becomes the solution of simultaneous ordinary differential equations on using the variational method. Its solution is easier than that of the finite-

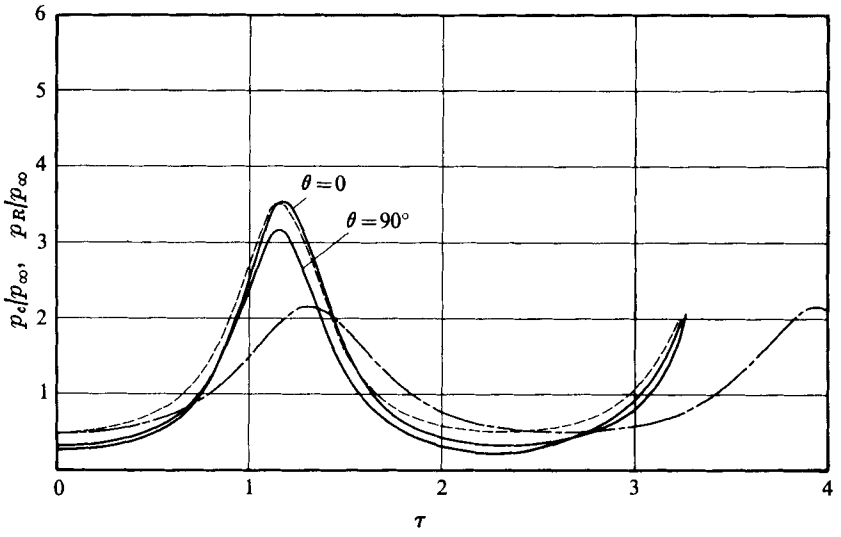

FIGURE 20. Pressure distributions on the bubble surface and gas pressures inside the bubble as functions of time. $p_{G0}/p_\infty = 0{\cdot}5$, $\gamma = 1{\cdot}4$. ——, p_R/p_∞, $T = 0{\cdot}1$; – – –, p_c/p_∞, $T = 0{\cdot}1$; —·—, p_c/p_∞, $T = 0$.

difference method, and the computing time is shorter. A finite expansion with spherical harmonics as the trial functions is used in our variational method. The convergence of the solution depends on the choice of trial function and the number ot terms in the expansion. If the number of terms in the expansion is increased and more reasonable trial functions are adopted, our method can compute the later stages of bubble collapse. In our method, it is easy to treat various boundary conditions. In particular, in a free boundary-value problem such as the motion of a bubble, the formulation of boundary conditions is straightforward and the computational program becomes compact. Thus, as shown in this paper, the surface tension and gas behaviour within the bubble are easily formulated.

The Chapman & Plesset method, based on the finite-difference procedure, requires numerous irregular meshes to obtain a good approximation of the bubble surface and therefore the computational time becomes large. Of course their method can treat the effect of surface tension, however it only adds a complicated term. As the mean radius of the bubble approaches zero, the convergence of the solution is doubtful. This occurs with the finite-difference method as well as with the variational method because the effect of surface tension excites higher-mode surface oscillation, so that instability of the solution may be introduced.

From these points of view, our variational method can provide easily and with good precision the information on the behaviour of a non-spherical bubble. We believe that this method will be very useful.

4. Conclusions

The following conclusions are drawn from the present study.

(i) The results obtained from numerical calculations performed by the variational method on the collapse of a non-hemispherical bubble attached to the solid wall are in

good agreement with those obtained by Chapman & Plesset (1972) for a similar problem. Therefore it may be considered that this variational method will give the same degree of accuracy as the finite-difference approximation used by them. The present method can readily be applied to complicated problems including the nonlinear effects. In the analysis of the collapse of a non-hemispherical bubble, however, it is difficult to simulate the collapse up to a mean radius less than 0·2, because of the occurrence of unstable solutions.

(ii) The variation in the bubble shape during the collapse depends on the initial deformation from the hemispherical shape. In collapse with constant internal pressure, a bubble which is initially a prolate hemispheroid changes its shape into an oblate hemispheroid, and can form a jet striking the wall. If the initial bubble shape is an oblate spheroid, it changes into a 'bell' shape.

(iii) The effect of surface tension is to accelerate the collapse of a bubble and to increase the deformation of the bubble in the final stages of the collapse. For a bubble containing non-condensable gas, the surface tension causes the shape oscillation and contributes to the increases in velocity and pressure on the bubble surface.

(iv) The cushioning effect of the internal gas retards the collapse of a bubble. The jet is weakened if it forms at all, or the bubble will rebound.

(v) It is presumed that the jet plays an important role in the cavitation damage when a vapour bubble attached to a solid wall collapses. In the case of a gaseous bubble, it is not clear whether the jet performs the destructive action or not.

The authors wish to express their sincere thanks to Mr N. Miura and Miss M. Kumagai for their assistance in the present study.

REFERENCES

ANTON, I. & POPOVICIU, M. 1972 The behaviour of hemispherical bubbles generated by electric sparks. *Proc. 4th Conf. Fluid Machinery, Budapest*, p. 89.

BENJAMIN, T. B. & ELLIS, A. T. 1966 The collapse of cavitation bubbles and the pressure thereby produced against solid boundaries. *Phil. Trans.* A **260**, 221.

CHAPMAN, R. B. & PLESSET, M. S. 1972 Nonlinear effects in the collapse of a nearly spherical cavity in a liquid. *J. Basic Engng, Trans. A.S.M.E.* D **94**, 142.

HAMMITT, F. G., KLING, C. L., MITCHELL, T. M. & TIMM, E. E. 1970 Asymmetric cavitation bubble collapse near solid objects. *Univ. Michigan Rep.* UMICH 03371-6-1.

HSIEH, D. Y. 1972 On the dynamics of nonspherical bubbles. *J. Basic Engng, Trans. A.S.M.E.* D **94**, 655.

KORNFELD, M. & SUVOROV, L. 1944 On the destructive action of cavitation. *J. Appl. Phys.* **15**, 495.

MITCHELL, T. M. & HAMMITT, F. G. 1973 Asymmetric cavitation bubble collapse. *J. Basic Engng, Trans. A.S.M.E.* I **95**, 29.

NAUDÉ, C. F. & ELLIS, A. T. 1961 On the mechanism of cavitation damage by nonhemispherical cavities collapsing in contact with a solid boundary. *J. Basic Engng, Trans. A.S.M.E.* D **83**, 648.

NUMACHI, F. 1958 Kavitationsblasen und Ultraschallwellen am Tragflügelprofil. *Forsch. Ing.-Wes.* **24**, 125.

PLESSET, M. S. 1954 On the stability of fluid flows with spherical symmetry. *J. Appl. Phys.* **25**, 96.

PLESSET, M. S. & CHAPMAN, R. B. 1971 Collapse of an initially spherical vapour cavity in the neighbourhood of a solid boundary. *J. Fluid Mech.* **47**, 283.

PLESSET, M. S. & MITCHELL, T. P. 1955 On the stability of the spherical shape of a vapor cavity in a liquid. *Quart. Appl. Math.* **13**, 419.

POPOVICIU, M. 1972 A photographic study of spherical bubbles dynamics. *Proc. 4th Conf. Fluid Machinery, Budapest*, p. 1031.

RATTRAY, M. 1951 Perturbation effects in cavitation bubble dynamics. Ph.D. thesis, California Institute of Technology.

RAYLEIGH, LORD 1917 On the pressure developed in a liquid during the collapse of a spherical cavity. *Phil. Mag.* **34**, 94.

SHIMA, A. 1968 The behavior of a spherical bubble in the vicinity of a solid wall. *J. Basic Engng, Trans. A.S.M.E.* D **90**, 75.

SHUTLER, N. D. & MESLER, R. B. 1965 A photographic study of the dynamics and damage capabilities of bubbles collapsing near solid boundaries. *J. Basic Engng, Trans. A.S.M.E.* D **87**, 511.

SMITH, R. H. & MESLER, R. B. 1972 A photographic study of the effect of an air bubble on the growth and collapse of a vapour bubble near a surface. *J. Basic Engng, Trans. A.S.M.E.* D **94**, 933.

TIMM, E. E. & HAMMITT, F. G. 1971 Bubble collapse adjacent to a rigid wall, a flexible wall, and a second bubble. *A.S.M.E. Cavitation Forum*, p. 18.

YEN, H. C. & YANG, W. J. 1968 Dynamics of bubbles moving in liquids with pressure gradient. *J. Appl. Phys.* **39**, 3156.